

## Double side read-out technique for mitigation of radiation damage effects in $\text{PbWO}_4$ crystals

This content has been downloaded from IOPscience. Please scroll down to see the full text.

2016 JINST 11 P04021

(<http://iopscience.iop.org/1748-0221/11/04/P04021>)

View [the table of contents for this issue](#), or go to the [journal homepage](#) for more

Download details:

IP Address: 134.83.1.241

This content was downloaded on 19/04/2016 at 09:43

Please note that [terms and conditions apply](#).

## Double side read-out technique for mitigation of radiation damage effects in PbWO<sub>4</sub> crystals

M.T. Lucchini,<sup>a,1</sup> E. Auffray,<sup>a</sup> A. Benaglia,<sup>a</sup> F. Cavallari,<sup>e</sup> D. Cockerill,<sup>d</sup> A. Dolgoplov,<sup>j</sup>  
J.L. Faure,<sup>m</sup> N. Golubev,<sup>h</sup> P.R. Hobson,<sup>l</sup> S. Jain,<sup>i</sup> M. Korjik,<sup>g</sup> V. Mechinski,<sup>g</sup> A. Singovski,<sup>b</sup>  
T. Tabarelli de Fatis,<sup>c</sup> I. Tarasov<sup>k</sup> and S. Zahid<sup>l</sup>

<sup>a</sup>European Organization for Nuclear Research, CERN,  
Geneva, CH-1211 Switzerland

<sup>b</sup>University of Minnesota,  
3 Morrill Hall 100 Church St. S.E., Minneapolis, MN, 55455 U.S.A.

<sup>c</sup>University of Milano-Bicocca,  
Piazza dell'Ateneo Nuovo 1, Milano, 20125 Italy

<sup>d</sup>STFC Rutherford Appleton Laboratory,  
Harwell Campus, Didcot, OX110QX United Kingdom

<sup>e</sup>INFN Sezione di Roma and Sapienza Università di Roma,  
P.le Aldo Moro 2, Roma, 00185 Italy

<sup>g</sup>Research Institute for Nuclear Problems, Byelorussian State University,  
Bobruiskaya str. 11, Minsk, 220030 Belarus

<sup>h</sup>Institute for Nuclear Research, Russian Academy of Sciences,  
60th October Anniversary pr. 7A, Moscow, 117312 Russia

<sup>i</sup>National Central University,  
No. 300, Zhongda Rd., Zhongli District, Taoyuan City, 32001 Taiwan

<sup>j</sup>Fermi National Accelerator Laboratory,  
Wilson Street & Kirk Road, Batavia, IL, 60510 U.S.A.

<sup>k</sup>Helmholtzzentrum für Schwerionenforschung GmbH, GSI,  
Planckstraße 1, Darmstadt, 64291 Germany

<sup>l</sup>Brunel University, Kingston Ln,  
Uxbridge, Middlesex, UB8 3PH United Kingdom

<sup>m</sup>Centre d'étude de Saclay, CEA/IRFU,  
Orme des Merisiers, Gif-sur-Yvette, 91191 France

E-mail: [marco.toliman.lucchini@cern.ch](mailto:marco.toliman.lucchini@cern.ch)

<sup>1</sup>Corresponding author.

**ABSTRACT:** Test beam results of a calorimetric module based on  $3 \times 3 \times 22 \text{ cm}^3$   $\text{PbWO}_4$  crystals, identical to those used in the CMS ECAL Endcaps, read out by a pair of photodetectors coupled to the two opposite sides (front and rear) of each crystal are presented. Nine crystals with different level of induced absorption, from 0 to  $20 \text{ m}^{-1}$ , have been tested using electrons in the 50–200 GeV energy range. Photomultiplier tubes have been chosen as photodetectors to allow for a precise measurement of highly damaged crystals. The information provided by this double side read-out configuration allows to correct for event-by-event fluctuations of the longitudinal development of electromagnetic showers. By strongly mitigating the effect of non-uniform light collection efficiency induced by radiation damage, the double side read-out technique significantly improves the energy resolution with respect to a single side read-out configuration. The non-linearity of the response arising in damaged crystals is also corrected by a double side read-out configuration and the response linearity of irradiated crystals is restored. In high radiation environments at future colliders, as it will be the case for detectors operating during the High Luminosity phase of the Large Hadron Collider, defects can be created inside the scintillator volume leading to a non-uniform response of the calorimetric cell. The double side read-out technique presented in this study provides a valuable way to improve the performance of calorimeters based on scintillators whose active volumes are characterized by high aspect ratio cells similar to those used in this study.

**KEYWORDS:** Calorimeter methods; Calorimeters; Radiation damage to detector materials (solid state); Radiation-hard detectors

---

## Contents

<b>1</b>	<b>Introduction</b>	<b>1</b>
<b>2</b>	<b>Double side read-out technique</b>	<b>2</b>
<b>3</b>	<b>Experimental setup and procedure</b>	<b>4</b>
3.1	Calorimetric module	4
3.2	The beam line	5
3.3	The experimental procedure	5
<b>4</b>	<b>Results</b>	<b>6</b>
4.1	Shower fluctuations	6
4.2	Calibration procedure	7
4.3	Energy reconstruction and linearity	9
4.4	Improvement of energy resolution in damaged crystals	11
4.5	Comparison with simulation	12
4.6	Measurement of light collection efficiency	14

---

## 1 Introduction

The performance of most of calorimeters based on scintillators as active material, can be strongly influenced by the spatial non-uniformity of light collection efficiency. If the probability of scintillation light to be collected at the photodetector varies at different points inside the volume of the calorimetric cell, a variation of the whole detector response occurs and the energy resolution is degraded. Calorimeters are usually designed to reduce as much as possible the contribution of light collection non-uniformity to the energy resolution. However, high radiation environments, such as those in which detectors will have to operate during the High Luminosity phase of the Large Hadron Collider (HL-LHC) [1, 2], can create defects inside the scintillator reducing its transparency to scintillation light and therefore reducing the light collection efficiency. As a consequence, the total light collection efficiency and its uniformity inside the crystal is strongly modified.

This mechanism was studied in detail for the case of the CMS Electromagnetic Calorimeter (ECAL) [3]. In this particular case, extremely high fluences of hadrons create stable defects inside the volume of  $\text{PbWO}_4$  crystals [4–6] leading to a strong degradation of its energy resolution to electromagnetic showers due to the change in light collection efficiency [7]. A similar influence of the light collection uniformity to the calorimeter performance can occur in sampling calorimeters based on scintillating fibers due to their high aspect ratio and finite attenuation length [8].

In this work, we investigate a possible way to mitigate these effects by means of a double side read-out (DRO) technique. In such configuration an additional photodetector is positioned on the front face of the crystals to allow the simultaneous detection of scintillation light at the two opposite

ends of the crystal. A beam test was performed at the CERN SPS North Area, using electrons in the 50–200 GeV energy range. The calorimetric module used for this test was made of nine PbWO<sub>4</sub> crystals with different level of hadron damage corresponding to induced light absorption coefficients  $\mu_{\text{ind}}$  ranging from 0 to 20 m<sup>-1</sup>. The results obtained in this test provide useful information for a better understanding of radiation damage effects in PbWO<sub>4</sub> crystals and represent an important validation of the Geant4 simulation tool used to model the evolution of crystal performance due to radiation damage. The experimental methods and the results achieved are discussed in the following sections.

## 2 Double side read-out technique

With respect to the standard CMS ECAL read-out of PbWO<sub>4</sub> crystals, in which a photodetector is coupled to the rear face of the crystal [3], the DRO technique exploits the additional information provided by a photodetector positioned on the front face of the crystal as shown in figure 1. For each incident electron, the shower produces the largest amount of scintillation photons close to the average shower maximum,  $t_{\text{max}} \propto \ln(E)$ , which for electrons of 50 and 200 GeV energy in PbWO<sub>4</sub> is respectively around 6.5 and 7.5 cm distant from the crystal front face. However, due to the stochastic nature of shower development the position of  $t_{\text{max}}$  fluctuates on an event-by-event basis. This fluctuation affects the average light path which scintillation photons have to travel to reach the photodetector, and therefore light gets more or less attenuated depending on the location of  $t_{\text{max}}$ . In a read-out configuration using single photodetector, these fluctuations are responsible for the degradation of energy resolution observed in damaged crystals due to the non-uniform light collection efficiency [7]. In a DRO configuration, the simultaneous read-out at the front and rear face signals provides a tool to estimate the position of  $t_{\text{max}}$  and to correct for its fluctuations on an event by event basis.

A Geant4 simulation [9] was used to investigate the effect of shower maximum fluctuations on the amount of light detected at the two opposite faces of damaged crystals. The tapered geometry of the crystals and their scintillation properties have been properly taken into account [3]. Different levels of light absorption, ranging from  $\mu_{\text{ind}} = 0$  to  $\mu_{\text{ind}} = 20$  m<sup>-1</sup> have been simulated. An example of the light collection efficiency curves  $\varepsilon_{\text{LC}}$ , namely the probability for scintillation light produced at a given position in the crystal to be collected at the photodetector, is shown in figure 1 for a crystal with  $\mu_{\text{ind}} = 10$  m<sup>-1</sup>.

The signals detected at the front ( $F_{sh}$ ) and rear ( $R_{sh}$ ) photodetectors, corresponding to an electron of energy  $E$  developing a shower in a crystal with absorption coefficient  $\mu$  can be written as:

$$F_{sh} = K_f \int E_{dep}(E, z) \varepsilon_f(\mu, z) dz \quad (2.1)$$

$$R_{sh} = K_r \int E_{dep}(E, z) \varepsilon_r(\mu, z) dz \quad (2.2)$$

where  $\varepsilon_f$  and  $\varepsilon_r$  are respectively the light collection efficiency curves for the front and rear photodetectors, and  $K_f$ ,  $K_r$  are calibration coefficients which take into account the photodetectors quantum efficiency and gain.

As shown in figure 1, showers from 50–200 GeV electrons develop their maximum closer to the front photodetector. Hence, light reaching the rear crystal face is more attenuated with respect

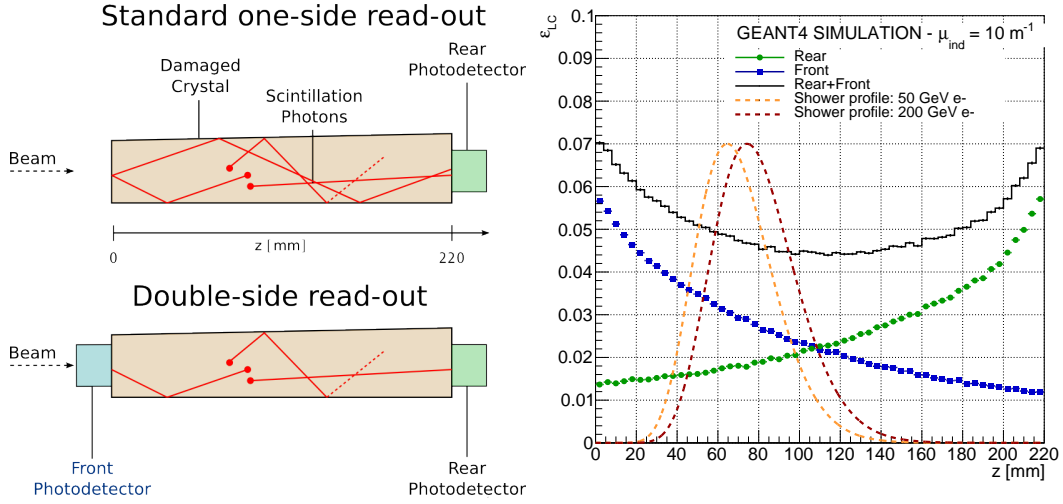


**Figure 1.** Left: schematic representation of the standard single read-out (top) and double side read-out configuration (bottom). Right: Geant4 simulation curves of light collection efficiency for front (color), rear (color) and double (color) read-out, for a crystal with  $\mu_{\text{ind}} = 10 \text{ m}^{-1}$ . Average shower profile of electrons with energy of 50–200 GeV is also shown.

to the light detected at the front face. Conversely, the energy resolution is worse for the front photodetector than for the rear one since  $t_{\text{max}}$  fluctuates in a region where  $\varepsilon_f$  is steeper than  $\varepsilon_r$  causing larger variations of the response.

The signals of front and rear detectors can be combined to obtain after intercalibration according to:

$$S_{\text{sum}} = \frac{K_r \cdot F_{sh} + K_f \cdot R_{sh}}{K_f K_r} = \int E_{dep}(E, z) \varepsilon_{\text{dro}}(\mu, z) dz. \quad (2.3)$$

In this case, the slope of the resulting light collection efficiency curve  $\varepsilon_{\text{dro}} = \varepsilon_f + \varepsilon_r$  is less steep than the individual curves  $\varepsilon_f, \varepsilon_r$ . As a consequence the overall response to electrons, obtained with the DRO configuration, is less affected by the light collection degradation and therefore the energy resolution is less degraded with respect to a single read-out configuration.

The signal reconstructed using eq. (2.3) improves the energy resolution due to the more uniform slope of  $\varepsilon_{\text{dro}}$  but is still affected by longitudinal shower fluctuations. To fully exploit the potential of the DRO technique the ratio of front and rear photodetector signals can be used to estimate the average position of the shower on the  $z$  axis and to apply an event-by-event correction.

This can be achieved by using an exponential approximation of the light collection efficiency curves such that  $\varepsilon_f = \exp(-\mu z)$  and  $\varepsilon_r = \exp(-\mu(L - z))$ , where  $L = 22 \text{ cm}$  is the length of the crystal. For a shower with maximum development,  $t_{\text{max}}$ , at the position  $z$ , a correction to the front and rear signals equals to  $1/\varepsilon_f$  and  $1/\varepsilon_r$  respectively should be applied to eliminate the effect of light collection non-uniformity. The combined signal can then be written as:

$$S_{\text{dro}} = F \cdot e^{\mu z} + R \cdot e^{-\mu(z+L)}. \quad (2.4)$$

Since both  $\mu$  and  $z$  are unknown variables, we can use the relation

$$\sqrt{\frac{R}{F}} = e^{\mu(z-L/2)} \quad (2.5)$$

in eq. (2.4) to obtain:

$$S_{\text{dro}} = k_{\mu} \left[ F \cdot \sqrt{\frac{R}{F}} + R \cdot \sqrt{\frac{F}{R}} \right] = 2k_{\mu} \sqrt{FR} \quad (2.6)$$

where  $k_{\mu} = \exp(\mu L/2)$  is an overall calibration constant and the ratio of the front and rear signals provides the event-by-event correction. The signal reconstructed with eq. (2.6) additionally reduces the fluctuations due to longitudinal shower development with respect to eq. (2.3).

The beam test study presented in the following provides a measurement of the experimental curves  $\varepsilon_f$ ,  $\varepsilon_r$  for a large range of absorption coefficients and provides the proof-of-principle for a double side read-out (DRO) technique. The crystal performance results obtained with the signal reconstructed using eq. (2.3) and eq. (2.6) are compared and discussed in section 4.

### 3 Experimental setup and procedure

#### 3.1 Calorimetric module

The calorimetric module consisted of nine  $\text{PbWO}_4$  tapered crystals of  $3 \times 3 \times 22 \text{ cm}^3$  identical to those used in the CMS ECAL Endcaps (EE) [3]. The crystals were inserted in a standard EE alveolar structure to form a  $3 \times 3$  array as shown in figure 2. The two crystals in position 0 and 5, were irradiated by placing them in the forward region of the CMS detector for few months [7]. The remaining crystals were irradiated with 24 GeV protons at the CERN PS facility [10], to various fluences between  $2.1 \times 10^{13}$  and  $1.3 \times 10^{14} \text{ cm}^{-2}$ . These levels of radiation correspond to the predicted charged hadron fluences in the ECAL Endcaps at pseudorapidity  $\eta = 2.6$  respectively at the end of the LHC and High Luminosity LHC operations [1, 2]. A non-irradiated crystal was placed in the centre of the matrix as a reference. The values of  $\mu_{\text{ind}}$  reported in figure 2 represent the average  $\mu_{\text{ind}}$  measured just before the beam test.

The alveolar structure was surrounded by 1 cm thick copper plates with pipes for the water circulation which allowed for the thermal stabilization of the crystals within  $0.2 \text{ }^\circ\text{C}$ . With respect to previous beam tests [7], some mechanics have been added to allow individual mounting of PMTs on the front side of the crystals and to provide a small pressure of the PMT against the crystal. An optical grease with refractive index 1.45 was used between crystal and PMT to improve the light extraction. A set of 18 Hamamatsu Photonics R5380 PMTs with bialkali photocathodes and borosilicate glass windows of 20 mm diameter were used to read out the light from both sides of each crystal [16]. Photomultiplier tubes have been chosen as photodetectors, instead of vacuum phototriodes as used in the CMS Electromagnetic Calorimeter, because of their high gain and low noise which allow a precise measurement given the low amount of light collected from highly damaged crystals.

The module, including the cooling and light monitoring system, was mounted inside a light tight aluminium box providing thermal isolation (figure 2). The box was installed on a remotely-controlled  $x - y$  table with a displacement range of  $\pm 30 \text{ cm}$  and positioning accuracy of  $\sim 1 \text{ mm}$ .

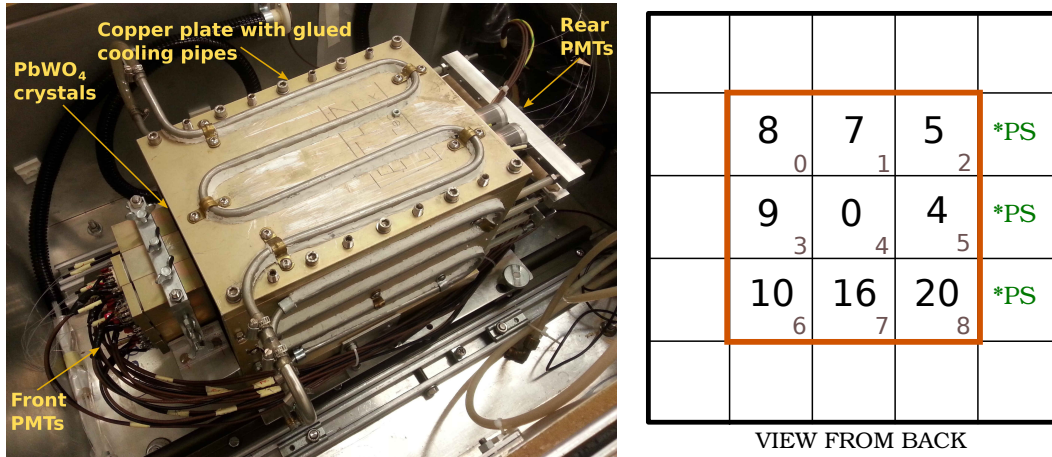


**Figure 2.** Left: picture of the experimental box, containing the 9 crystals read-out by front and rear face simultaneously. Right: arrangement of irradiated crystals inside the alveolar structure of the calorimetric module. Black number in the centre of each crystal represent the corresponding  $\mu_{\text{ind}}$  whereas the grey number in the corner is the channel number. The three crystals on the right side, marked as “PS”, were used as pre-shower for transverse configuration measurements discussed in section 4.6.

### 3.2 The beam line

The experiment was performed at the CERN SPS North Area H4 beam line which provides an electron beam in the 50 GeV to 200 GeV range with hadron and muon contamination below 0.2%. The incoming beam particles were detected by a set of four scintillation counters used to trigger the data acquisition. The impact of the beam particles on the crystal matrix was obtained by extrapolating their trajectory measured using two sets of beam hodoscopes. Each set was composed of two planes of 64 scintillating fibres of square cross-section  $0.5 \times 0.5 \text{ mm}^2$ , read out by a multi-anode PMT. Each plane provides, respectively, a measurement of the electron position in the  $x$  and  $y$  directions with a resolution better than  $200 \mu\text{m}$  [12].

The signals from the PMTs, beam counters and hodoscopes were delivered to the counting room, located about 60 m from the beam zone, by coaxial cables and digitized by a 12-bits VME LeCroy Charge Analog-to-Digital Converter (ADC) [13]. The integration time was set to 300 ns to accommodate the PMT pulse length and channel-to-channel transition time variation in the long coaxial cable connecting PMT output and ADC input.

### 3.3 The experimental procedure

As a first step, the box was centered to have the beam incident on the central non-irradiated crystal. In this configuration a large statistic run was taken using 100 GeV electrons. The variation of the crystal response as a function of impact point due to shower transverse leakage is shown in figure 3 as measured by the rear PMT, for the  $x$ - and  $y$ -axis. A fit of these containment distributions was used to calculate the centre of the calorimetric module with respect to the coordinate frame of the hodoscopes as described in [7].

After the position of each crystal was determined, the high voltage of each PMT was adjusted such that the peak from a 100 GeV electron shower corresponded to  $\sim 1200$  ADC counts in each

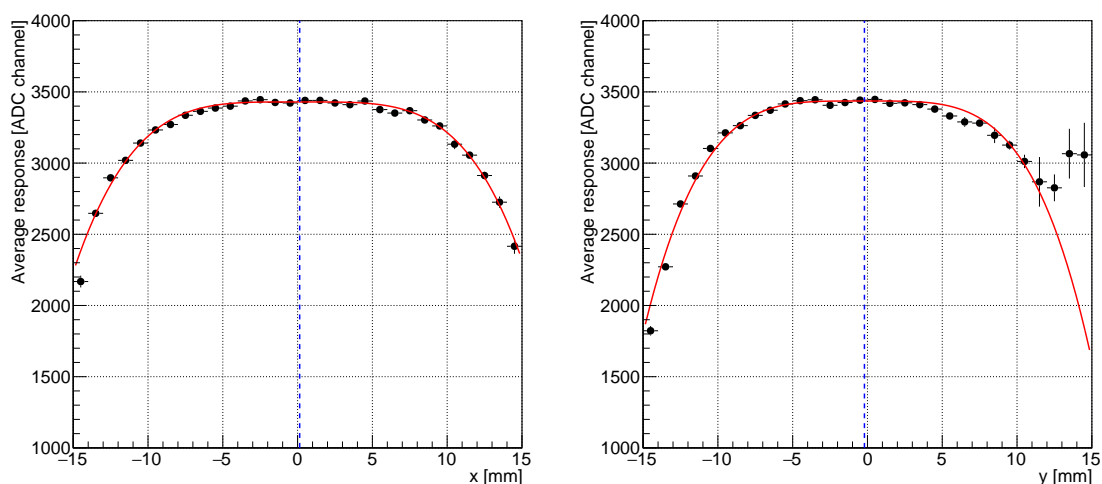


**Figure 3.** Containment distributions, obtained with 100 GeV electrons impinging on the central non-irradiated crystals, representing the variations of crystal response due to transverse shower leakage as a function of electron impact point on  $x$  (left) and  $y$  (right) axis. Red line represents the fit function  $A \cdot (x - x_0)^4 + B$  and the blue dashed line the crystal centre estimation.

crystal. This setting allowed the use of the same PMT gain for the whole energy scan in the 50–200 GeV range.

Once the high voltages of all PMTs were set, energy scans were performed with the beam incident on the centre of each crystal for 50, 100, 150 and 200 GeV electrons. As a last step, the whole box containing the calorimetric module was rotated by 90 degrees anti-clockwise in order to have the beam striking on the lateral side of the crystals. This configuration enabled to perform a scan of the crystal response along the  $z$ -axis providing a direct measurement of the light collection efficiency curves as discussed in section 4.6.

## 4 Results

### 4.1 Shower fluctuations

The longitudinal profile of energy deposition for electromagnetic showers, and so the position of shower maximum  $t_{\max}$  fluctuates due to the stochastic processes involved in the shower development. If the response of the crystal is uniform along the longitudinal axis, as it is the case for non-irradiated  $\text{PbWO}_4$  crystals, this fluctuation does not affect the signal measured by the photodetector. However, this is not the case for highly damaged crystals in which the strongly non uniform light collection efficiency along the crystal axis causes a smearing of the detected signal related to shower fluctuations.

As described in section 2, the double side read-out technique is based on the assumption that the light signal sharing between front and rear photodetectors is correlated to the longitudinal fluctuations of the shower development. In a non-irradiated crystal, having a rather uniform efficiency of light collection along its  $z$ -axis, regardless of the position where the shower maximum

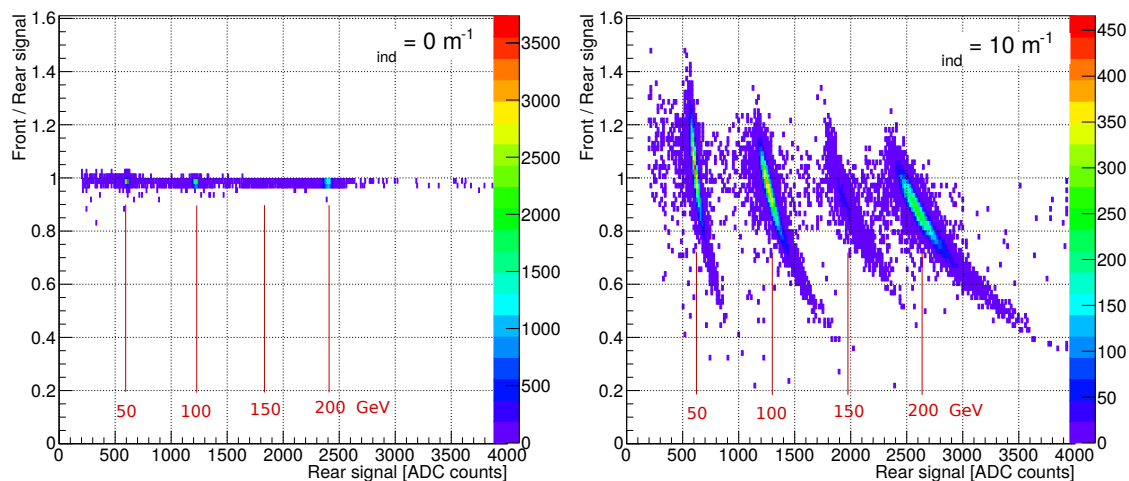


**Figure 4.** Correlation between the front/rear signal ratio and the signal measured at the rear photodetector at different energies (50, 100, 150 and 200 GeV). For the non-irradiated crystal (left) there is no change in the ratio between front and rear photodetector signals whereas for a damaged crystal with  $\mu_{\text{ind}} = 10 \text{ m}^{-1}$  (right) the event-by-event fluctuations in the shower longitudinal development are responsible for large variations in the front/rear signal ratio.

develops, the light detected at both photodetectors is identical. Conversely, as soon as the light absorption,  $\mu_{\text{ind}}$ , of the crystal increases due to radiation damage, the ratio of the front and rear signals starts to be affected by the fluctuations in the shower maximum position. This effect has been clearly observed in figure 4, where for  $\mu_{\text{ind}} = 0$  the front/rear ratio remains unchanged over the whole electron energy range and event by event fluctuations of the signal are minimal while for a damaged crystal with  $\mu_{\text{ind}} = 10 \text{ m}^{-1}$ , the ratio of the two photodetector signals shows strong variation for a fixed electron energy.

It has to be noticed that longitudinal shower fluctuations are always present (also in non-irradiated crystals) but their effects can be observed and thus corrected only in damaged crystals, as discussed later in section 4.4. The right plot in figure 4 shows the basic mechanism of the double read-out correction.

## 4.2 Calibration procedure

Before combining the front and rear signal according to eq. (2.6) the two photodetectors of each crystal have to be intercalibrated, i.e. the coefficients  $K_f$  and  $K_r$  must be obtained. Given the multiplicity of factors affecting each photodetector response, this task is not straightforward. The intercalibration coefficients include variations in the response mostly related to the different high voltages and thus different amplification gain of the two PMTs. These coefficients also take into account for channel-by-channel response variations due to photocathode quantum efficiency and crystal-to-PMT optical coupling.

The standard calibration procedure used in previous beam tests [7], uses the inverse of the position of amplitude distribution peak corresponding to 50 GeV electrons, as intercalibration coefficient. Using the same technique to intercalibrate the front and rear photodetectors would lead

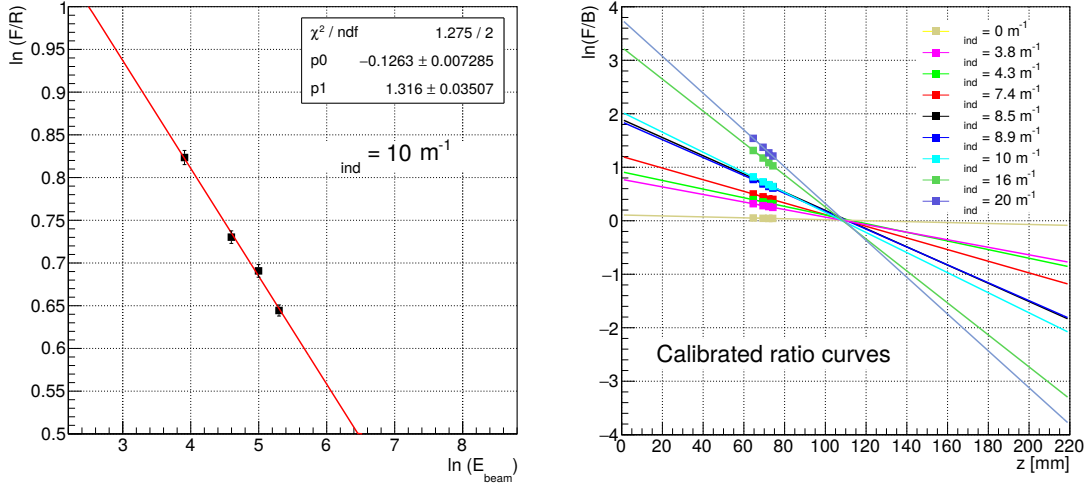


**Figure 5.** Left: correlation between the ratio of front/rear signal and beam energy for the crystal with  $\mu_{\text{ind}} = 10 \text{ m}^{-1}$  before intercalibration of photodetectors. Right: curves representing the drift of shower maximum position after photodetectors intercalibration. The slope of each curve is related to the  $\mu_{\text{ind}}$  of the corresponding crystal.

to an equal response of the two PMTs to 50 GeV electrons. Such calibration would be correct for non-irradiated crystals but imprecise for crystals with  $\mu_{\text{ind}} > 0$ . Indeed, according to figure 1, the response of the front PMT for a crystal with  $\mu_{\text{ind}} = 10 \text{ m}^{-1}$  should be  $\sim 1.5$  times higher with respect to the rear one due to the difference between  $\varepsilon_f$  and  $\varepsilon_r$  around the corresponding shower maximum position ( $\sim 7 \text{ cm}$ ).

In the following we describe an intercalibration procedure which is valid for any value of  $\mu_{\text{ind}}$  and is independent of the beam energy. This approach is based on the shift of the average position of the shower max  $t_{\text{max}}$  as a function of beam energy:

$$t_{\text{max}} = X_0(4.2 + 1.8 \times \ln(E)) \quad (4.1)$$

where  $X_0 = 0.89 \text{ cm}$  for  $\text{PbWO}_4$ . The drift of  $t_{\text{max}}$  towards the rear face of the crystal, when beam energy increases from 50 to 200 GeV, can be related to the change in the ratio of front/rear signal. Using an exponential approximation for the light collection efficiency curves, and assuming they are symmetric with respect to the centre of the crystal, the ratio of eq. (2.1) and (2.2) yields:

$$\frac{F_{sh}}{R_{sh}} = \frac{K_f}{K_r} \cdot \frac{e^{-\mu z}}{e^{-\mu(L-z)}} \quad (4.2)$$

where  $L = 22 \text{ cm}$  is the crystal length. The following linear relation can be obtained:

$$\ln\left(\frac{F_{sh}}{R_{sh}}\right) = -2\mu z + \mu L - \ln\left(\frac{K_r}{K_f}\right). \quad (4.3)$$

Equation 4.3 is used to fit the experimental data as shown in the left plot of figure 5.

The average ratio of front and rear signal decreases due to the shift of shower maximum towards the rear face at high energies. To obtain the intercalibration coefficients  $K_f$  and  $K_r$  it is sufficient

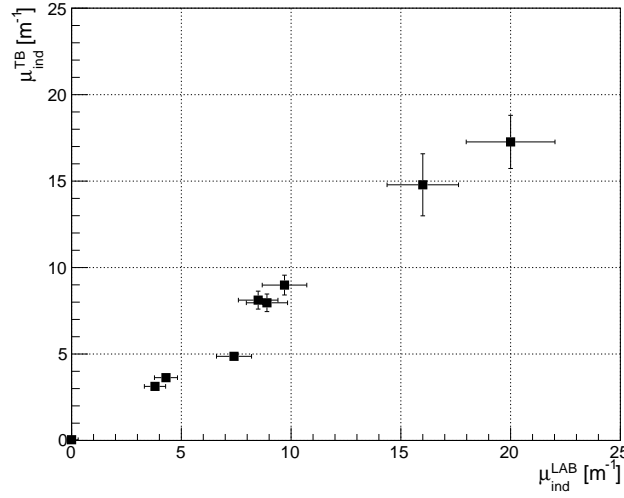


**Figure 6.** Correlation between the values of the effective induced absorption measured with test beam data  $\mu_{\text{ind}}^{\text{TB}}$  and the values of  $\mu_{\text{ind}}^{\text{LAB}}$  obtained from direct light transmission measurement in laboratory fitted with a linear function (red line).

to convert beam energy into  $t_{\text{max}}$  using eq. (4.1) and requiring the front and rear signals to be identical when shower maximum is located at  $z = L/2 = 110$  mm. This leads to the condition  $\ln(F_{sh}/R_{sh}) = 0$ . Under such condition, eq. (4.3) yields the intercalibration coefficients for each pair of photodetectors. By construction, after this calibration the shower maximum curves for each crystal intersecates at  $z = 110$  mm as visible in the right plot of figure 5. Their slope is proportional to the value of  $\mu_{\text{ind}}$  of each crystal according to eq. (4.3). This indirect measurement of the induced absorption for each crystal shows a good correlation with the values of  $\mu_{\text{ind}}$  measured in laboratory, as reported in section 3.

However, the estimate of induced absorption coefficients measured with direct light beam  $\mu_{\text{ind}}^{\text{LAB}}$  represents the attenuation of light traveling a straight path inside the crystal. The absorption coefficient measured in this beam test  $\mu^{\text{TB}}$  correspond to the effective attenuation of scintillation light emitted isotropically and thus traveling a longer average path before reaching the photodetector. To evaluate the light absorption induced by radiation damage using test beam data we define:

$$\mu_{\text{ind}}^{\text{TB}} = \mu^{\text{TB}} - \mu_0^{\text{TB}} \quad (4.4)$$

where  $\mu_0^{\text{TB}} = (0.44 \pm 0.04) \text{ m}^{-1}$  represents the intrinsic absorption of the central non-irradiated crystal and  $\mu^{\text{TB}}$  the absorption coefficients of irradiated crystals. A comparison of light induced absorption from laboratory measurements,  $\mu_{\text{ind}}^{\text{LAB}}$ , and test beam data,  $\mu_{\text{ind}}^{\text{TB}}$ , is reported in figure 6 and the observed correlation is a confirmation of the calibration procedure based on eq. (4.3).

### 4.3 Energy reconstruction and linearity

In the following analysis a beam spot selection of  $4 \times 4 \text{ mm}^2$  around the centre of each crystal was used in order to minimize the effect of transverse shower leakage. After intercalibration, a comparison between the amplitude distributions of front and rear photodetectors and their sum

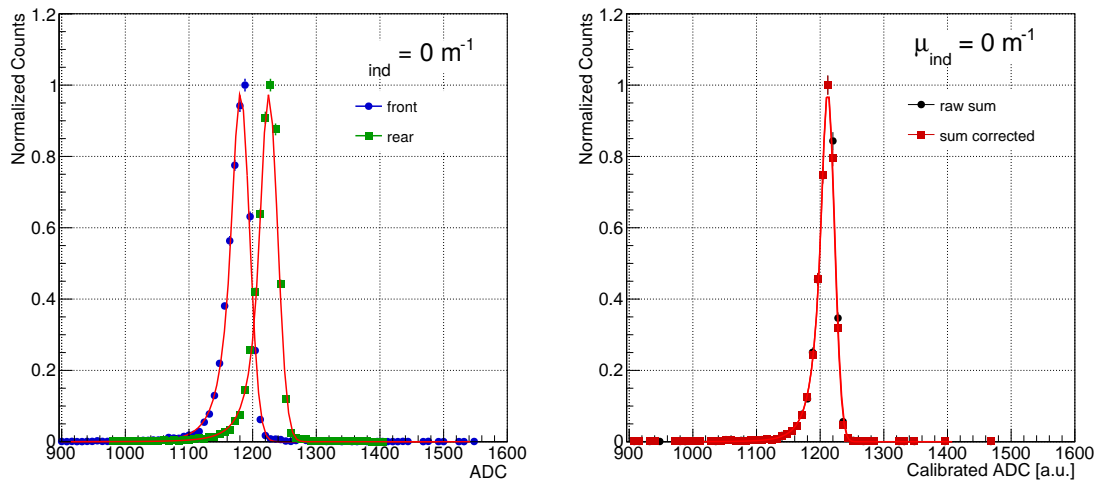


**Figure 7.** Energy distributions of a non-irradiated crystal corresponding to 100 GeV electrons for a single read-out configuration (left) and for the combined double read-out signal (right) using eq. (2.3) (raw sum) and eq. (2.6) (sum corrected).

(eq. (2.6)) has been made. The distributions obtained for 100 GeV electrons beam are shown in figure 7 for a non-irradiated crystal and in figure 8 for a damaged crystal with  $\mu_{\text{ind}} = 10 \text{ m}^{-1}$ . As expected, no change in the shape of the distribution is observed for a non-irradiated crystal. Conversely, for damaged crystals the energy distribution obtained from the combination of front and rear signal is narrower than those from single read-out. The non-gaussian tails are also removed resulting in a more gaussian-like distribution. It can also be noticed that the distribution for front photodetector signal is wider than the rear one, due to the slope of  $\varepsilon_f$  being steeper than  $\varepsilon_r$  around shower maximum position.

The response of different crystals has been studied for the electron energies of 50, 100, 150 and 200 GeV. The amplitude distributions were fitted using a Crystal Ball [15] function to take into account for the asymmetric tails and the most probable value was used as estimator for the crystal response  $S(E_b)$  at a given beam energy  $E_b$ . The *linearity*,  $L(E_b)$ , of the crystal response can be written as:

$$L(E_b) = \frac{S(E_b)}{E_b} \cdot \frac{50}{S(50)}. \quad (4.5)$$

The linearity curves for a non-irradiated crystal and for the crystal with  $\mu_{\text{ind}} = 10 \text{ m}^{-1}$  are reported in figure 9. These curves enable the non-linearities of the response related to the increase of  $\mu_{\text{ind}}$  in each crystal for different read-out configuration (i.e. front PMT, rear PMT and combined DRO sum) to be studied. The linearity of a non-irradiated crystal for each read-out configuration is flat within  $\sim 1\%$ . The small decrease in the measured signal at high energies is attributed to longitudinal shower leakage. In damaged crystals the non-linear behavior of the rear signal, up to  $\sim 12\%$  for a  $\mu_{\text{ind}} = 10 \text{ m}^{-1}$ , confirms the observations of previous beam tests [7]. The non-linearity of the front signal, being in the opposite direction with respect to the rear one, was never observed before but is consistent with the interpretation given in previous publication [7] and discussed in section 2.

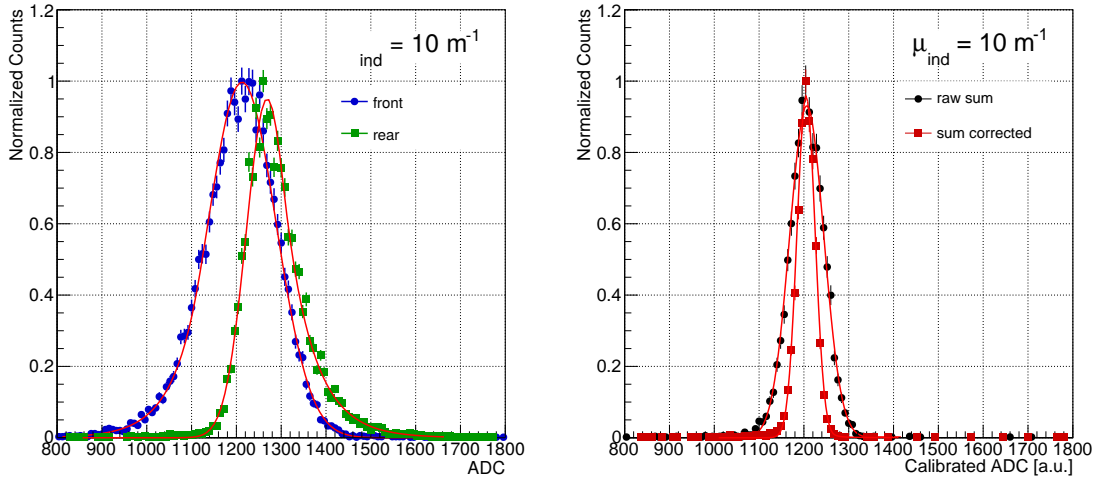


**Figure 8.** Energy distributions of a damaged crystal ( $\mu_{\text{ind}} = 10 \text{ m}^{-1}$ ) corresponding to 100 GeV electrons for a single read-out configuration (left) and for the combined double read-out signal (right) using eq. (2.3) (raw sum) and eq. (2.6) (sum corrected).

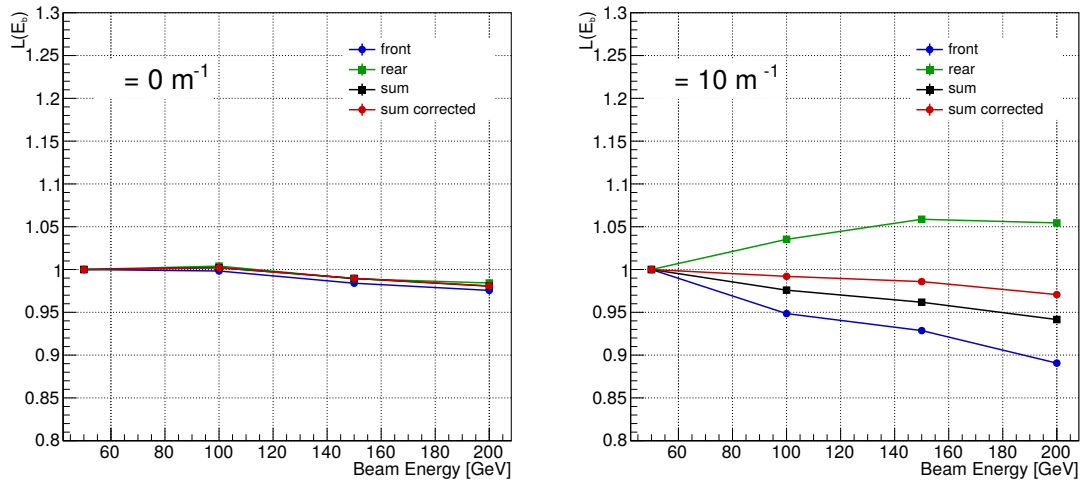


**Figure 9.** Linearity curves normalized to 50 GeV for the non-irradiated crystal (left) and for a damaged crystal with  $\mu_{\text{ind}} = 10 \text{ m}^{-1}$ . Different read-out configuration are shown: front photodetector (blue squares), rear photodetector (green dots), raw sum given by eq. (2.3) (black) and corrected sum given by eq. (2.6) (red).

A first important feature of the double read-out configuration can be noticed in the linearity curve of the combined DRO response. The non-linear behavior of damaged crystals is strongly mitigated and the response becomes more uniform over the 50–200 GeV energy range, similar to non-irradiated crystal.

#### 4.4 Improvement of energy resolution in damaged crystals

As previously anticipated, the main advantage of a double read-out configuration for damaged crystals, is the mitigation of the energy resolution degradation due to increased non-uniformity of

light collection efficiency. Neglecting longitudinal shower leakage at high energies, the energy resolution of a calorimeter, as in the case of the CMS ECAL, can be parameterized using the formula:

$$\frac{\sigma_E}{E} = \sqrt{\left(\frac{A}{\sqrt{E}}\right)^2 + \left(\frac{B}{E}\right)^2 + C^2} \quad (4.6)$$

where  $A$  represents the stochastic term,  $C$  the constant term and  $B$  the contribution from the electronic noise. The value of  $B$  has been fixed for each channel using the corresponding noise estimated from the pedestals and varied between 170 MeV and 340 MeV. To disentangle the contribution of the noise to the resolution of a given crystal, the value of  $B$  estimated from the pedestal of each channel, has been subtracted in quadrature from the corresponding  $\sigma(E)/E$ :

$$\frac{\sigma_E}{E} = \sqrt{\left(\frac{A}{\sqrt{E}}\right)^2 + C^2}. \quad (4.7)$$

To take into account the tails of the energy distributions, the  $\sigma_{\text{eff}}$ , defined as half of the minimum interval containing 68% of the amplitude distribution, is used in the following as an estimator of the energy resolution. The results are shown in figure 10 for a non-irradiated crystal and a damaged crystal with  $\mu_{\text{ind}} = 10 \text{ m}^{-1}$ . The energy resolution at energies above 50 GeV is mainly dominated by the constant term. For the non-irradiated crystal the constant term is found to be  $C = 1.06 \pm 0.03\%$ , dominated by the partial transverse shower containment in a single  $\text{PbWO}_4$  crystal ( $\sim 84\%$ ). For the damaged crystal ( $\mu_{\text{ind}} = 10 \text{ m}^{-1}$ ) poorer energy resolution is observed, as expected, for the front read-out configuration. With respect to the standard rear read-out only ( $C = 4.7 \pm 0.1\%$ ), we observed a mitigation of the constant term down to  $C = 2.8 \pm 0.10\%$  with the un-corrected combined signal of eq. (2.3) and further improvements when the DRO-correction of eq. (2.6) is applied leading to a constant term of  $C = 1.4 \pm 0.1\%$ . Similar results are obtained for all the crystals, even at high levels of  $\mu_{\text{ind}} = 16\text{--}20 \text{ m}^{-1}$ , and are compared with the predictions from the Geant4 simulation discussed in section 4.5.

#### 4.5 Comparison with simulation

An intrinsic absorption coefficient of  $\mu_{\text{int}} = (0.2 \pm 0.1) \text{ m}^{-1}$ , estimated from laboratory measurements, was used for the simulation of the non-irradiated crystal. Such value is slightly smaller than the  $\mu_0^{\text{TB}}$  obtained using test beam data in eq. (4.4). Such values are consistent with each other since the former represents the intrinsic absorption coefficient of a non-irradiated crystal whereas the latter also takes into account for the larger average path of isotropic light and surface effects. For such good light transmittance, the light collection efficiency of a non irradiated crystal is influenced by a “focusing” effect due to the tapered geometry [17]. This effect enhances the collection efficiency at the rear photodetector for photons produced close to the front crystal face. As a consequence the  $\varepsilon_r$  curve is not flat but shows a smooth slope. For the front read-out the focusing effect is opposite and leads to a steeper slope of  $\varepsilon_r$ . As a consequence the DRO correction cannot improve the constant term arising from non-uniform light collection efficiency curves in non-irradiated crystals. It is thus possible and consistent with both experimental measurements and simulation that the DRO configuration can lead to smaller constant term for slightly damaged crystals ( $\mu_{\text{ind}} = 1\text{--}6 \text{ m}^{-1}$ ) than for a non-irradiated one.

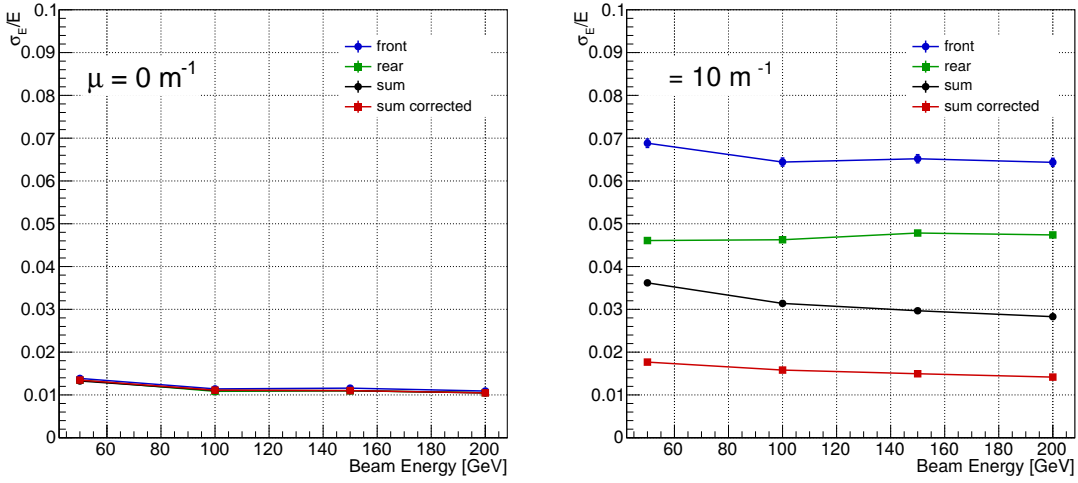


**Figure 10.** Energy resolution curves for the non-irradiated crystal (left) and for a damaged crystal with  $\mu_{\text{ind}} = 10 \text{ m}^{-1}$ . Different read-out configuration are shown: front photodetector (blue squares), rear photodetector (green dots), raw sum given by eq. (2.3) (black) and corrected sum given by eq. (2.6) (red).

The degradation of constant term due to radiation damage can be estimated by comparison with non-irradiated crystal according to:

$$\Delta C = \sqrt{C_i^2 - C_{\text{ni}}^2} \quad (4.8)$$

where  $C_{\text{ni}}$  and  $C_i$  are the constant term of non-irradiated and a damaged crystal respectively. In this way the effect on shower leakage to the constant term, common to all crystals, is removed. The constant term increases up to  $\sim 10\%$  for  $\mu_{\text{ind}} = 20 \text{ m}^{-1}$  in a single read-out configuration whereas it is mitigated to a level of 5.7% and 1.9% respectively for the combined DRO raw sum (eq. (2.3)) and the DRO corrected signal (eq. (2.6)). Comparison between the test beam data and the prediction from Geant4 simulation shows a good agreement as shown in the left plot of figure 11.

The non-linear response of damaged crystals can also be quantified with respect to the non-irradiated crystal as:

$$\Delta NL = \frac{S_i(200)}{S_i(50)} \cdot \frac{S_{\text{ni}}(50)}{S_{\text{ni}}(200)} \quad (4.9)$$

where  $S_i(200)$  and  $S_{\text{ni}}(200)$  are respectively the responses of a damaged and a non-irradiated crystal to electrons of 200 GeV energy. The increase of non-linearity,  $\Delta NL$ , in damaged crystals is reported in the right plot of figure 11 for different levels  $\mu_{\text{ind}}$ . For the most damaged crystal ( $\mu_{\text{ind}} = 20 \text{ m}^{-1}$ ) the  $\Delta NL$  is about 15% and decreases to  $\sim 10\%$  and below 1% for the combined DRO raw sum (eq. (2.3)) and the corrected DRO signal (eq. (2.6)) respectively.

A good agreement between the Geant4 simulation predictions and experimental data is observed for the increase of the non-linear response, as visible in the right plot of figure 11. This is an additional proof that the effects of damage inside  $\text{PbWO}_4$  crystals and the degradation of their calorimetric performance are well understood.

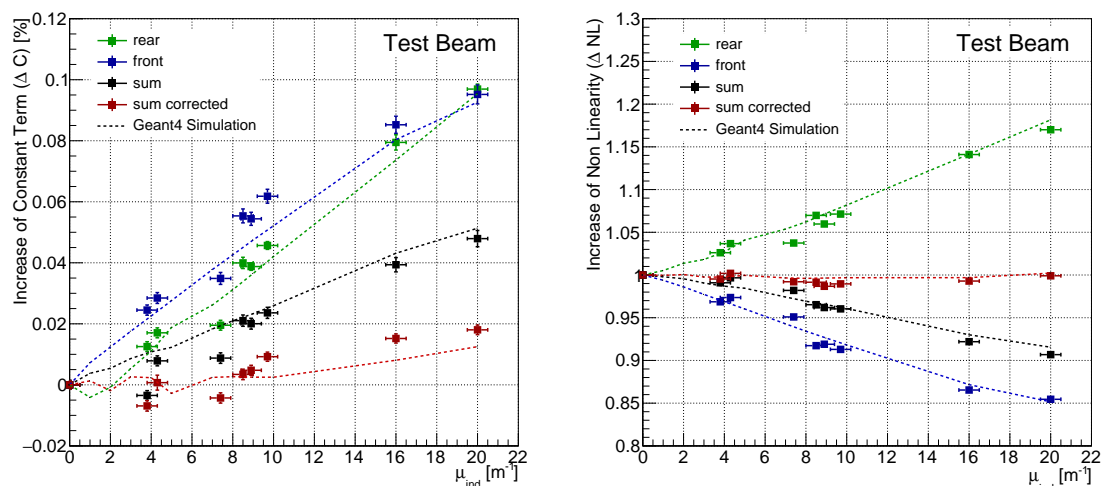


**Figure 11.** Left: the increase of constant term due to longitudinal non-uniformities of light collection efficiency is shown for different values of  $\mu_{ind}$  corresponding to the crystals used for this study (square dots). The degradation of constant term is shown for different read-out configurations and compared with predictions from the Geant4 simulation (dotted lines). Right: the increase of non-linearity due to longitudinal non-uniformities of light collection efficiency is shown, as a function of  $\mu_{ind}$ , for the crystals tested in this study (square dots). The increase of non-linearity is shown for different read-out configurations and compared with predictions from the Geant4 simulation (dotted lines).

#### 4.6 Measurement of light collection efficiency

As discussed in section 2, the double read-out technique aims to mitigate the degradation of energy resolution due to the increased non-uniformity of light collection efficiency in damaged crystals. In particular, the double read-out correction used to reconstruct the signal in eq. (2.6) is based on the assumption that light collection efficiency curves of irradiated crystals can be approximated by an exponential function. Therefore, it is of fundamental importance to provide an experimental measurement of such curves.

To measure the non-uniformity of light collection efficiency along the  $z$  axis of each crystal, the whole calorimetric module was rotated by 90 degrees. By gradually moving the table, a scan of the crystal response as a function of electron impact point along crystal length was made. In order to deposit a reasonable amount of energy in each crystal, in this configuration, an additional layer of 3  $PbWO_4$  crystals was positioned in the alveolar structure as shown in figure 2. Given the crystal tapered geometry [3], the shower will deposit a different amount of energy in each layer of crystal depending on the amount of “passive” material in front of it and on the crystal thickness at a given  $z$  position. This variation in energy deposition was simulated with Geant4 and correction coefficients, to be applied to the measured response, have been obtained. The energy deposited in each layer predicted by simulation is about 15, 25 and 20 GeV respectively for the first, second and third layer. The slope of the energy deposited along  $z$  shows variations up to  $\sim 15\%$  and is different for each layer.

The measured response of the front and rear PMTs for each channel, after the correction for the energy deposits, provides a measurement of the light collection efficiency curves  $\varepsilon_f$ ,  $\varepsilon_r$  of

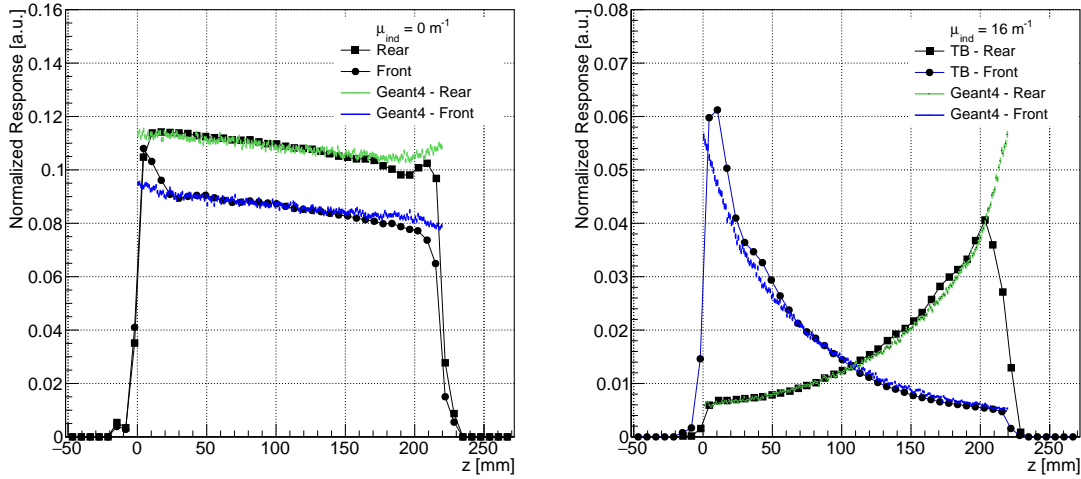


**Figure 12.** Comparison of experimental measurement of light collection efficiency curves (black dots) with Geant4 predictions (green and light blue line) for a non-irradiated crystal (left) and a damaged crystal with  $\mu_{\text{ind}} = 16 \text{ m}^{-1}$  (right).

the corresponding crystal. In figure 12 the experimental profiles of light collection efficiency are normalized to the simulation prediction and a good agreement between the slopes is observed. Close to the ends of the crystals, i.e. in the ranges 0–20 mm and 200–220 mm, light propagation is more sensitive to surface effects such as reflections at the alveolar structure-crystal boundary and quality of surface polishing. These effects are difficult to be modeled with accuracy and can explain the small discrepancy between data and simulation in these regions. However, the slope of light collection efficiency in proximity of the crystal ends is marginally affecting the degradation of energy resolution and linearity as the shower maximum occurs close to the crystal centre.

The efficiency curves for all the crystals used in this study are shown in figure 13 for both rear and front read-out. In the central part of the crystal, the light collection efficiency curves show an exponential behavior which is consistent with the assumption that light attenuation along crystal axis can be mostly attributed to bulk absorption.

The present result, provides useful information to better understand the radiation damage effects in  $\text{PbWO}_4$  crystals and represents the proof-of-concept of a double read-out configuration approach.

A calorimetric module made of nine  $\text{PbWO}_4$  crystals with different levels of hadron damage has been tested at CERN with electrons from 50 to 200 GeV. Each crystals was instrumented with a pair of PMTs to read out the light from both ends. This double side read-out (DRO) configuration has been proved to strongly mitigate the degradation of the energy resolution due to the increase of non-uniformity of light collection along the crystal length, due to radiation damage.

The results of this test prove that the degradation of the constant term of energy resolution can be reduced from 10% to 2.5% for strongly damaged crystals by means of a double side read-out of the scintillation light. In addition, the response of damaged crystals is restored back to a linear behavior by means of a proper combination of front and rear photodetector signals. A first measurement of the light collection efficiency curve degradation up to high levels of induced

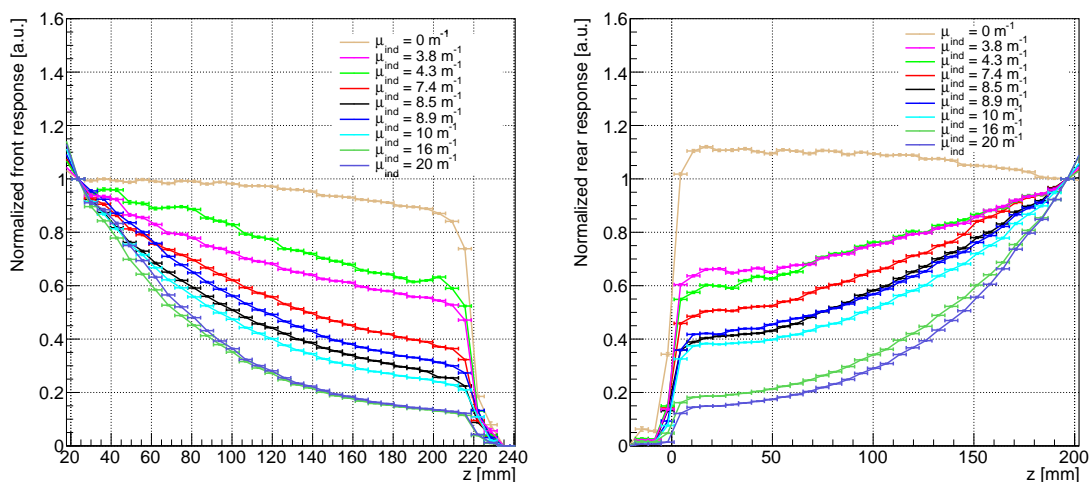


**Figure 13.** Light collection efficiency curves measured in test beam for all the nine crystals with different levels of induced absorption  $\mu_{\text{ind}}$ . Results are shown for the front (left) and rear (right) photodetector.

absorption,  $\mu_{\text{ind}} \sim 20 \text{ m}^{-1}$ , is also presented. The experimental results have been compared with expectations from a Geant4 simulation of the whole setup and a good agreement is observed.

## Acknowledgments

We would like to acknowledge the support from the CERN SPS North Area, in particular Adrian Fabich for his assistance in optimizing particles beam. We also thank Maurice Glaser and Federico Ravotti who have been responsible for the proton irradiation at the CERN PS IRRAD facility. We are grateful to the CMS ECAL collaboration for the support given to the present work.

## References

- [1] CMS collaboration, *Technical Proposal for the Phase-II Upgrade of the CMS Detector*, [CERN-LHCC-2015-010](#) (2015) [LHCC-P-008].
- [2] M. Lucchini et al., *Evolution of the response of the CMS ECAL and possible design options for calorimetry at the High Luminosity LHC*, *IEEE Nucl. Sci. Symp. Med. Imag. Conf.* (2013).
- [3] CMS collaboration, *The CMS electromagnetic calorimeter project: Technical Design Report*, [CERN-LHCC-97-033](#) (1997) [CMS-TDR-4].
- [4] M. Huhtinen, P. Lecomte, D. Luckey, F. Nessi-Tedaldi and F. Pauss, *High-energy proton induced damage in PbWO<sub>4</sub> calorimeter crystals*, *Nucl. Instrum. Meth. A* **545** (2005) 63.
- [5] P. Lecomte, D. Luckey, F. Nessi-Tedaldi and F. Pauss, *High-energy proton induced damage study of scintillation light output from PbWO<sub>4</sub> calorimeter crystals*, *Nucl. Instrum. Meth. A* **564** (2006) 164.
- [6] E. Auffray and A. Singovski, *Experimental Study of Lead Tungstate Scintillator Proton-Induced Damage and Recovery*, *IEEE Trans. Nucl. Sci.* **59** (2012) 2219.
- [7] T. Adams et al., *Beam test evaluation of electromagnetic calorimeter modules made from proton-damaged PbWO<sub>4</sub> crystals*, [2016 JINST 11 P04012](#).

- [8] M. Lucchini et al., *Test beam results with LuAG fibers for next-generation calorimeters*, *2013 JINST* **8** P10017.
- [9] GEANT4 collaboration, S. Agostinelli et al., *GEANT4: A Simulation toolkit*, *Nucl. Instrum. Meth. A* **506** (2003) 250.
- [10] M. Glaser, F. Ravotti and M. Moll, *Dosimetry assessments in the irradiation facilities at the CERN-PS accelerator*, *IEEE Trans. Nucl. Sci.* **53** (2006) 2016.
- [11] C. Furetta et al., *Fluence and dosimetric measurements for a  $\pi^\pm$  irradiation facility*, *Nucl. Phys. Proc. Suppl.* **B 44** (1995) 503.
- [12] J. Spanggaard, *Delay Wire Chambers — A Users Guide*, *SL-Note-98-023-BI* (1998) and online pdf version at <http://cds.cern.ch/record/702443/files/sl-note-98-023.pdf>.
- [13] *Charge Analog-to-Digital Converter*, <http://teledynelecroy.com/lrs/dsheets/1182.htm>.
- [14] National Instruments Corp., *LabVIEW System Design Software*, <http://www.ni.com/labview/>.
- [15] *ROOT. Data Analysis Framework*, <http://root.cern.ch/drupal/content/roofit>.
- [16] HAMAMATSU Photonics K.K. Electron tube division, *Photomultiplier tubes and assemblies for scintillating counters and high energy physics*, [http://neutron.physics.ucsb.edu/docs/High\\_energy\\_PMT\\_TPMO0007E01.pdf](http://neutron.physics.ucsb.edu/docs/High_energy_PMT_TPMO0007E01.pdf).
- [17] R. Chipaux and F.-X. Gentit, *Simulation of light collection in the CMS lead tungstate crystals with the program Litrani: Coating and surface effects*, *Nucl. Instrum. Meth. A* **486** (2002) 48.